



# Prediction and Analysis of Behaviour of Laterally Loaded Single Piles in Improved Gravel Soil

Guangming Yu<sup>1</sup> · Weiming Gong<sup>1</sup> · Meihe Chen<sup>1</sup> · Guoliang Dai<sup>1</sup> · Yuchen Liu<sup>1</sup>

Received: 8 September 2017 / Revised: 7 March 2018 / Accepted: 30 April 2018 / Published online: 6 December 2018  
© Iran University of Science and Technology 2018

## Abstract

To better understand the mechanism of development of lateral resistance of single drilled piles installed in improved soil profile. Side-by-side static load tests were performed on the piles installed in virgin soil profile and improved soil profile with the soil ahead of the pile cement-improved. Parametric three-dimensional finite element analyses were performed to study the effect of grouting radius. More soils at the side of piles make a critical contribution to resisting lateral loads due to the influence of improved soil ahead of the pile. A new hyperbolic  $p$ - $y$  function that modifies the initial subgrade modulus and the ultimate lateral soil resistance is proposed based on the finite element analyses to account for the effect of the cement improvement. The proposed  $p$ - $y$  method is capable of predicting laterally loaded pile response in cement-improved soil profiles as measured in the static load tests. The accuracy of the proposed  $p$ - $y$  model is appropriate as shown by comparing measured and calculated the lateral behaviour of the single pile.

**Keywords** Lateral load transfer method · Static load tests ·  $p$ - $y$  curve · Finite element modelling · Lateral soil resistance

## 1 Background

Pile foundations are commonly used to transfer external loads to soil medium without excessive deformations at the pile head. The lateral deformation of piles is a key factor to be considered in the design process. Various methods have been proposed to reduce the lateral movement of the foundations. For example, new types of foundation such as the caisson-piles composite foundation (CCPF) [1] and the root foundation [2] were used to improve the lateral bearing

capability and stiffness. Also, enlarging the diameter of the pile and adding extra piles have been adopted to solve these engineering practical problems. Nevertheless, these solutions are relatively costly.

An optimized alternative approach is to increase the stiffness and strength of subgrade soil. The Interest in improving the lateral resistance of piles by grouting technology has increased over the past two decades because it is a more cost-efficient approach compared with other treatment methods. Ashford et al. [3] studied the effect of ground improvement on the capacity of foundations in liquefiable sand. Rollins and Sparks [4, 5] analysed the improvement of soil resistance with compacted fill method. Rollins and Brown [6, 7] compared the effect of soil mixing and jet grouting for shallow ground treatment. Soltani et al. [8] acquired the  $p$ - $y$  curves of cement-improved soil around a single pile. Taghavi, Amirata [9, 10] studied  $p$ -multipliers in improved ground by varying soil stiffness and pile spacing.

---

✉ Weiming Gong  
wmgong@seu.edu.cn

Guangming Yu  
yuguangming@seu.edu.cn

Meihe Chen  
230169062@seu.edu.cn

Guoliang Dai  
daigl@seu.edu.cn

Yuchen Liu  
230159415@seu.edu.cn

<sup>1</sup> Key Laboratory of Concrete and Prestressed Concrete Structures of Ministry of Education, School of Civil Engineering, Southeast University, Sipailou #2, Nanjing 210096, China

## 2 Introduction

Design of laterally loaded piles often involves the consideration of complicated soil–structure interaction due to the highly non-linear behaviour of soil medium surrounding the

pile foundation. Researchers have performed plenty of studies on the lateral response of pile foundations via theoretical analyses [11] and field tests [3, 4]. Although the 3D numerical methods can estimate and predict well the mechanical response of laterally loaded piles when correct soil models and parameters are considered, they generally require the knowledge of constitutive models and relatively high computational cost, making it difficult to use in the design process of foundations. In contrast, the  $p$ - $y$  method is used widely to model the nonlinear behaviour of pile–soil interaction due to its simplicity and versatility. The notion of  $p$ - $y$  curves was originally proposed by Reese and Matlock [12] based on winkle elastic foundation beam theory [13]. Matlock [14] and Reese et al. [15] developed the  $p$ - $y$  approach based on experimental results of laterally loaded piles. Kim et al. [16] outlined a series of different expressions of the  $p$ - $y$  curves, such as hyperbolic function [17, 18], bilinear function [19], strain wedge model based on the wedge theory [20] among others [15, 21, 22].

This paper presents mechanical parameters of improved gravel soil that were back-calculated based on the field test in Luoyang city. The mechanism of lateral soil resistance improvement was analysed through a series of 3D FE analyses. Finally, a new lateral load-transfer curve is proposed to consider the effect of cement-improved gravel soil on the bearing capacity of a single pile. The proposed model was verified by the laterally loaded single model pile test.

### 3 Project Details and Field Tests

Field tests were conducted at the arch bridge site named New Street across the Luo River Bridge, which connects Luo Yang Old City with the New City. It consists of the south, north and a river channel section of the bridge. The main bridge is designed for an arch in the river channel section and its topside structure for nine span arches with a single arch span of 45–95 m. The substructure is a low-cap pile groups foundation which uses drilled piles construction technology. Its bridge floor width is 35.5 m, total length is 618 m. The pile groups consist of 23 bored concrete piles with a horizontal design load of 70,000 kN from the arch thrust at the pile cap. These piles have a diameter of  $D=2.0$  m and a length of  $L=35.0$  m (relative length  $L/D=17.5$ ). There are nine layers of soil around the piles. Figure 1 shows the particle size distribution of gravel soil. By evaluating the sieve analysis test data, it is found that the gradation of sand is poor with diameters of coarse grains mostly exceeding 0.5 mm.

In terms of arch structure, it has become increasingly common to limit the lateral deformation of the pile-group foundation at the cap. The arch bridge is a type of statically indeterminate structure bearing long-term horizontal thrust.

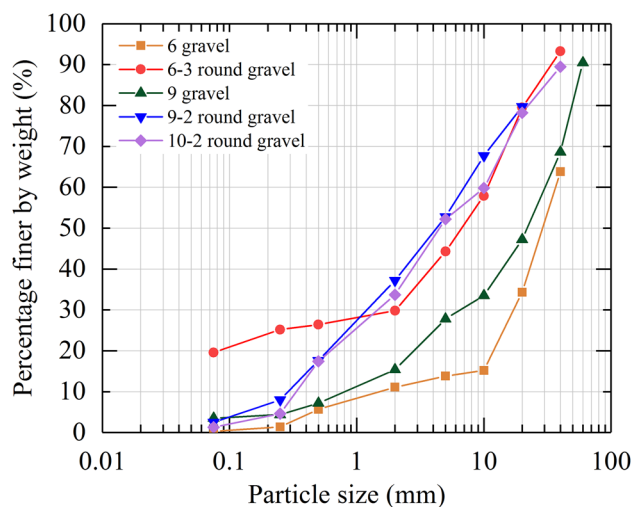


**Fig. 1** Grain size distribution of gravelly soils at the test site. **a** Structure diagram of grouting hole. **b** Structure diagram of steel flower tube

The lateral displacement of pile groups is likely to exceed the allowable limit and render arch axis of the main arch ring changed in the adjacent cross if piles have too much lateral load or if the subgrade lacks lateral soil resistance. As a result, the superstructure is split off from bridge foundation.

Piles' lateral bearing capacity is much higher than their vertical bearing capacity. However, pile foundations often need to be subjected to the lateral load. Previous research and analyses [12–15, 23] have suggested that soils in the shallow portion of the geological section have the greatest impact on lateral distortion and load transfer. The Chinese JGJ design code (JGJ94-2008) [15] recommends that the major influential depth of soil under pile's lateral load is  $2(D+1)$ . Thus, the shallow soil at the back of an engineering pile was improved in the depth of 6 m with cement by high-pressure jet grouting technique to solve the dearth of the lateral soil resistance of pile foundation. It is post-grouted treatment in the shallow soil around piles that can meet the requirement of practical engineering. There is a significant practical value to study lateral load-bearing properties of piles in cement-improved soil. Figure 2 shows grouting scheme. The area of grouted soil around pile is a half ring with 1.0 m in diameter away from the lateral sides of the pile.

The situ lateral load tests were conducted to inspect the effect of grouting with large horizontal jacks for a pile in improved soil and another pile in virgin soil. The distance between the two piles poured with C30 concrete was  $3.3D$  in the static lateral load test. For this lateral load test, the load was applied from 300 to 1500 kN with the increment of 150 kN. Figure 3 shows the arrangement for two piles subjected to side-by-side lateral loads.

**Fig. 2** Grouting scheme: **a** structure diagram of grouting hole and **b** structure diagram of steel flower tube

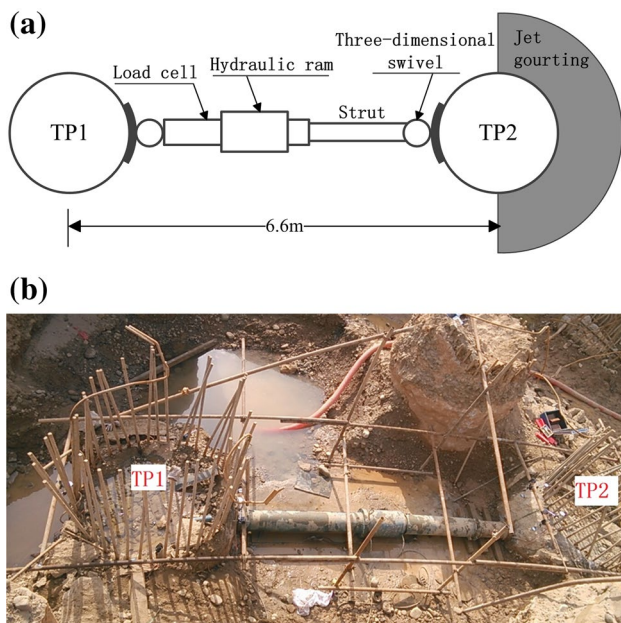
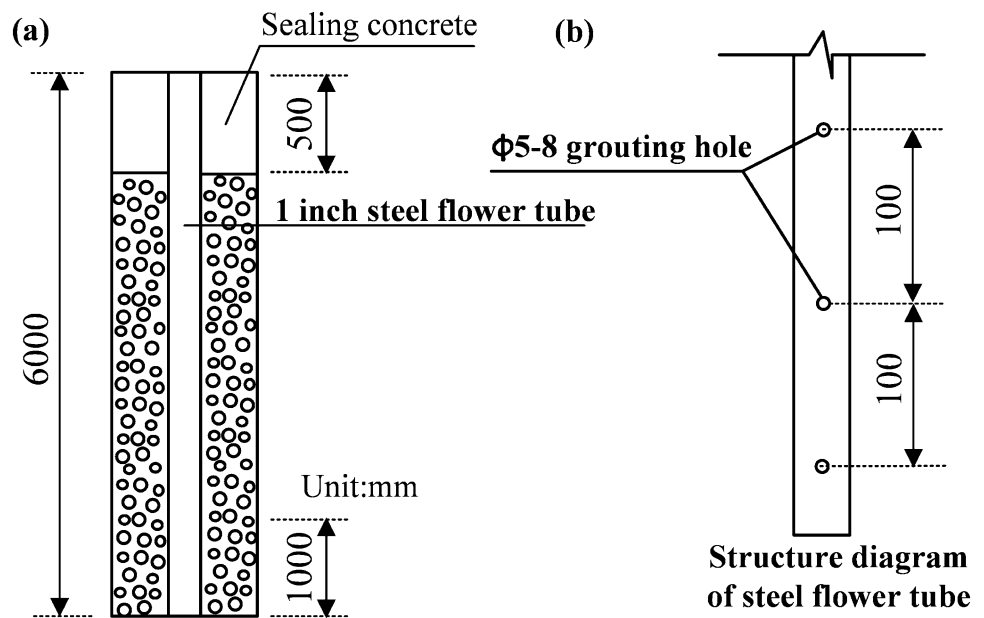


**Fig. 3** Arrangement for two piles simultaneously under two-direction lateral loading. **a** Plan view, **b** field test

## 4 Numerical Analysis of the Field Test

### 4.1 Finite Element Mesh, Boundary Conditions and Modelling Procedure

The 3D finite element model comprised the pile, grouting soil and virgin soils. A DXF format file containing geometrical information of the pile-soil model can be imported directly into soil explore of PLAXIS3D version

2016. Then the model was assigned physical and mechanical property to calculate the behaviour of single piles installed in the soil grouted.

The soil volume in the PLAXIS program is modelled by means of 10-node tetrahedral elements which have three local coordinates. This type of element provides a second-order interpolation of displacements. Volume pile is better than embedded beam structural element to reflect characteristics of laterally loaded pile. Figure 4 illustrates the 464, 41 elements and 66,185 nodes 3D finite mesh in the analysis. At the bottom of the model, the displacements were set to zero in the three directions,  $x$ ,  $y$ , and  $z$ . The vertical boundaries of model were free in the  $z$ -direction and fixed in the  $x$ - and  $y$ -directions. Considering the influence of boundary effects on pile's mechanical behavior mentioned in [24–26], the bottom elevation and the horizontal sides of the computational domain were taken far enough from the single pile to exclude its effect. More specifically, the model boundaries comprise a width of 7.5 times the pile diameter ( $D$ ) from the pile centre and a height of 1.71 times the pile length ( $L$ ) below the pile-head level.

### 4.2 Constitutive Model and Model Parameters

It is particularly critical that a correct constitutive model is implemented in the numerical analysis to reflect the soil behaviour under given load conditions. The stiffness of a pile is much higher than one of soil. Therefore, the response of the laterally loaded pile is considered as a linear elastic model with a Young's modulus of 25 GPa. A point worth emphasizing is that an elastic material was used to model soilcrete by Rollins and Brown [7] because

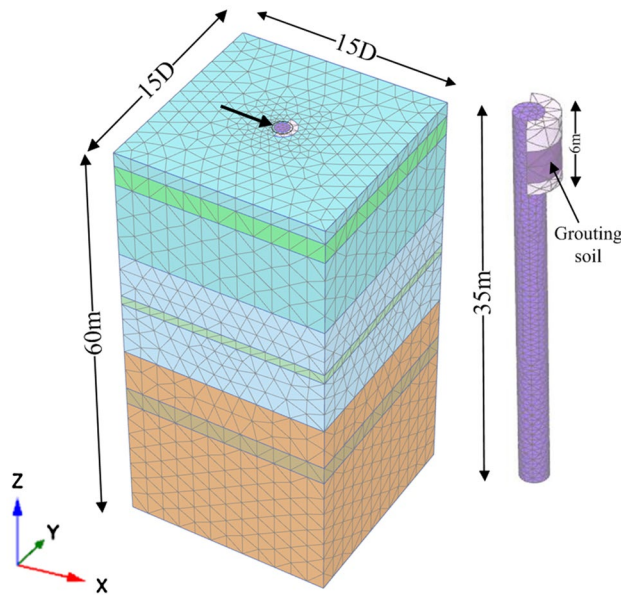


**Fig. 4** Three-dimensional FE model of laterally loaded pile in grouting soil

the soilcrete has a much higher strength than the clay. However, its strength remains much lower than one of a pile, large deformation of a pile also results in failure of jet grouting soil. It is appropriate that a non-associated Mohr–Coulomb model was used to model grouting soil and virgin soil. The drained type is employed to simulate the drained behaviour of grouting soil and virgin soil. The parameters of the linear elastic model and the Mohr–Coulomb model are listed in Table 1. It summarizes the values of soil parameters calculated through the back-analysis iterative process.

### 4.3 Parameters Back-Analysis

The pile has a length of 35 m, a slenderness ratio of 17.5 and the lateral load at pile head is considered to apply on the ground surface. Poulos and Davis [27] proposed a

**Table 1** Material parameters used for FE analysis (arch bridge site)

Layer	Model	$\gamma_{\text{sat}}$ (kN/m <sup>3</sup> )	$E_s$ (MPa)	$\mu_s$	$\varphi$ (°)
⊙Gravel	M.C	21.2	69	0.27	33
⊙-3Round gravel	M.C	20.0	51	0.30	27
⊙Gravel	M.C	21.6	86	0.25	35
⊙-2Round gravel	M.C	20.8	62	0.29	30
⊙Gravel	M.C	22.0	40	0.20	38
⊙-2Round gravel	M.C	21.0	30	0.27	32
Pile	L.E	25.0	25,000	0.20	–

M.C. Mohr–Coulomb-elasto-plastic model, L.E linear-elastic model

method to classify piles in different categories based on the flexibility factor  $K_r$ , see Eq. (1):

$$K_r = \frac{E_p I_p}{E_s L_p^4}, \quad (1)$$

$K_r \geq 0.1$ : rigid piles.

$0.01 \leq K_r < 0.1$ : relative stiff piles.

$0.001 \leq K_r < 0.01$ : medium flexible piles.

$1 \times 10^{-4} \leq K_r < 0.001$ : flexible piles.

$1 \times 10^{-5} \leq K_r < 1 \times 10^{-4}$ : very flexible piles.

With  $E_p I_p$  the section stiffness of the pile,  $L_p$  its embedded length and  $E_s$  the soil secant modulus (or deformation modulus). In the following,  $E_p I_p = 2.35 \times 10^{10}$  N m<sup>2</sup> and  $L_p = 35$  m. It is found that deformation modulus is in the range of 16.34–36 MPa. Therefore, the flexibility factor falls in the range from  $4.35 \times 10^{-4}$  to  $9.6 \times 10^{-4}$  and the pile in the FEM model can be classified as flexible.

As is shown in Fig. 5 that illustrates the lateral load vs. pile-head deformation curves. There is a good agreement between calculated and measured results of piles in virgin soil and improved soil. Table 2 summarizes values of improved Luoyang gravel soil's parameters calculated by the back-analysis method. The result reveals that the stiffness and strength of gravel soil can be improved by jet grouting technique [28].

According to back-analysis of soil parameters improved by grouting technique, four groups of the analysis model's grouting radius vary from 0 to 3 m in the unilateral range of the pile. These models were established to explore the effect of the range of cement-improved gravel soil on the nonlinear behaviour of laterally loaded piles. Figure 6 reflects the ground profile information and the range of grouting soil.

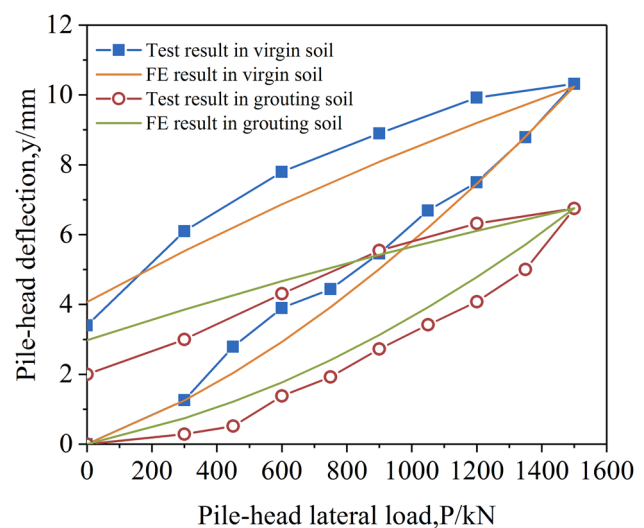


**Fig. 5** Comparison of measured and calculated lateral load vs. displacement at the head of piles

**Table 2** Material parameters of improved gravel soil

Layer	Model	$\gamma_{sat}$ (kN/m <sup>3</sup> )	$E_s$ (MPa)	$\mu_s$	$c$ (kPa)	$\varphi$ (°)
ⓐgrouting gravel	M.C	21.2	234.6	0.27	19	40
ⓑ-3grouting round gravel	M.C	20.0	172	0.30	19	40

### 5 Analysis of Influential Scope of Soil in Horizontal Direction

A displacement of 10 mm was applied at the single pile head to acquire the horizontal influential scope of virgin soil and improved soil which has a ring grouting radius of 1 m. Figure 7 shows several sectional horizontal views of lateral displacement  $u_x$  of soil at several depths  $z$  ( $0D$ ,  $1D$ ,  $2D$  and  $3D$ ). It is assumed in [29] that the soil displacement below 20% of the deformation at the pile top is the influential range of soil around a pile in the free face.

Table 3 shows the increasing ratio of horizontal influential scope before and after soil grouted. In the plane of  $z=0D$ , the soil’s horizontal influential range is  $1.75D$  behind the pile,  $2.45D$  ahead of the pile, and only  $1.1D$  at the sides of the pile in virgin soil, while they are extended by the increment of 10%, 18% and 36% under the condition of soil cement-improved, respectively. The similar growth regularity can also be seen in other depths after soil grouted, except beyond  $3D$  depth where the single pile does not almost make an effect on the soil around it.

The jet grouting gravel soil on the front of the pile provides lateral resistance with better integrity than virgin soil does because its cohesion and friction angle are increased. The greatest influential area is located at the side of the pile than ahead or behind it under the circumstance of improved

gravel soil. More soils at the side of the pile are pushed into the area resisting lateral loads by soils ahead of the pile after cement-improved. On the contrary, it can be neglected that the role of improved gravel soil on expanding the area of soils behind the pile. There exists the gap between the pile and the soil behind the pile when it happens lateral displacement forward the load orientation.

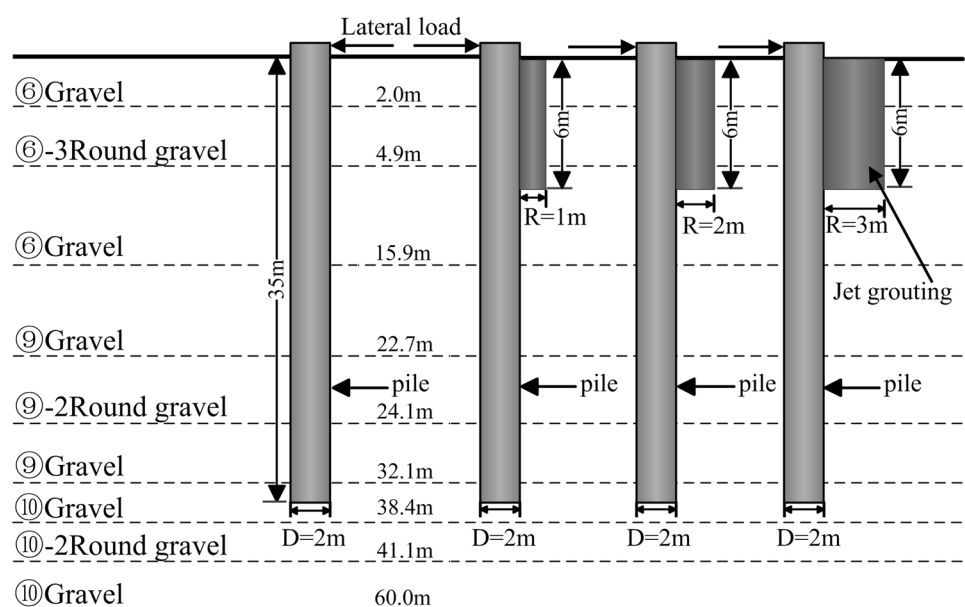
### 6 Development of Modified $p$ - $y$ Curves

#### 6.1 Derivation of Soil Resistance $p$

The soil resistance  $p$  can be deduced by double differentiation of bending moments or first-order derivative of shear force extracted from results of numerical analysis. Generally, the former is used to obtain lateral soil resistance for experimental results, while the latter is for numerical simulation to improve accuracy of derivation. Among the various curve fitting techniques, piecewise polynomial approximation, global polynomial approximation, quintic spline approximation and cubic spline interpolation, were the most commonly recommended [30]. To mathematically define the polynomial correctly, it is critical to decide the degree and order of a polynomial.

Firstly, a 9th order polynomial equation was employed to describe the profile of shear force from analysis results

**Fig. 6** Elevation view for grouting range in finite analysis



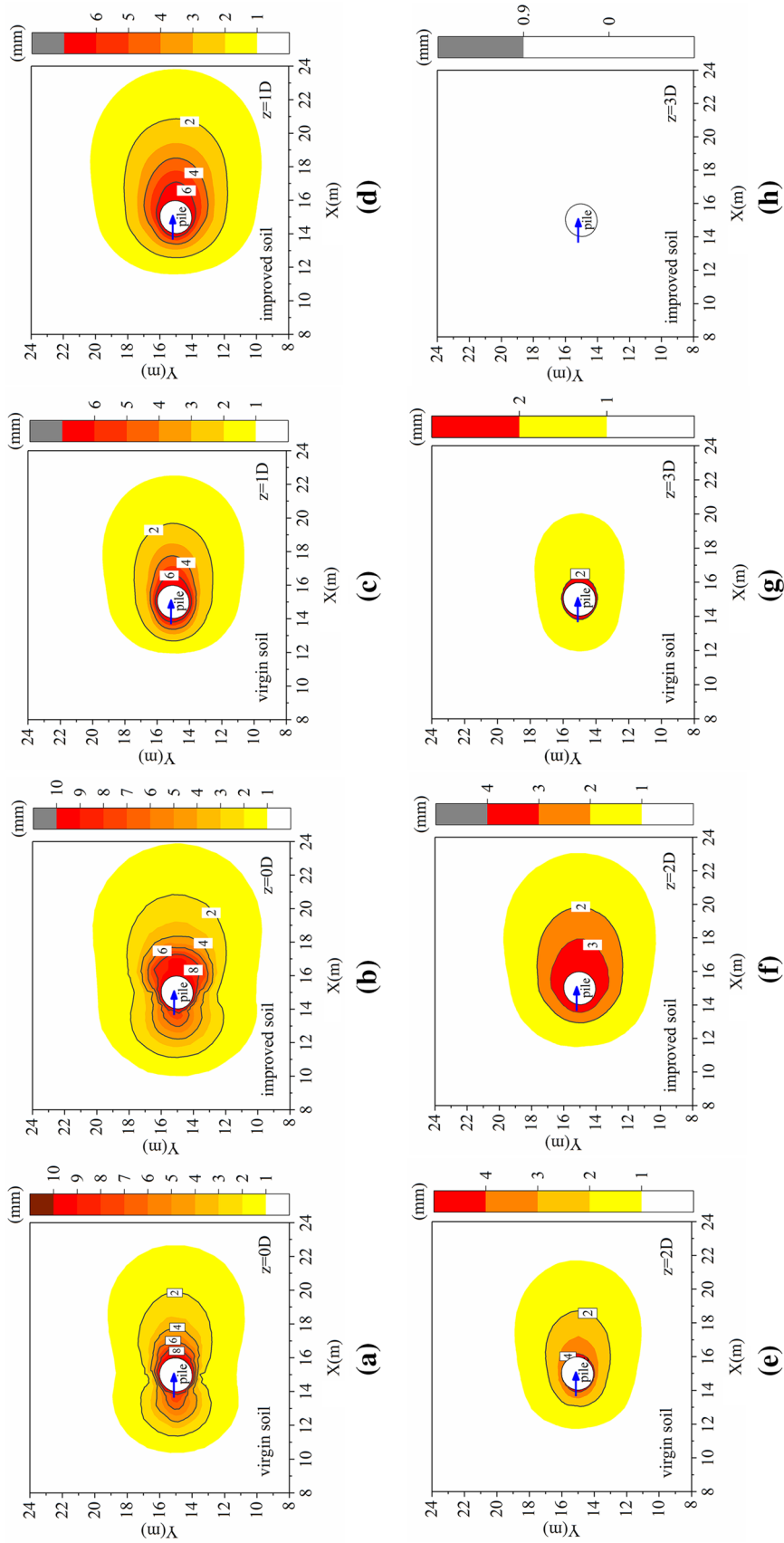


Fig. 7 Horizontal influence scope of soil for virgin soil and improved soil at various depths

**Table 3** Increasing ratio of horizontal influence scope

Depth	Soil condition	Area at side of pile	Area ahead of pile	Area behind pile
$z=0D$	Virgin	$1.1D$	$2.45D$	$1.75D$
	Improved	$1.5D$	$2.9D$	$1.95D$
	Increasing ratios	1.36	1.18	1.1
$z=1D$	Virgin	$1.25D$	$2.35D$	$1.2D$
	Improved	$1.6D$	$2.9D$	$1.2D$
	Increasing ratios	1.28	1.23	1.0
$z=2D$	Virgin	$1D$	$1.85D$	$1D$
	Improved	$1.35D$	$2.4D$	$1D$
	Increasing ratios	1.35	1.30	1.0
$z=3D$	Virgin	$0.55D$	$0.75D$	$0.6D$
	Improved	$0D$	$0D$	$0D$
	Increasing ratios	–	–	–

by the method of least squares. The Eq. (2) is presented as follows:

$$V = a_9z^9 + a_8z^8 + a_7z^7 + a_6z^6 + a_5z^5 + a_4z^4 + a_3z^3 + a_2z^2 + a_1z + a_0, \tag{2}$$

where  $a_0, a_1, \dots, a_9$  are undetermined coefficients.

Secondly, the first-order differential of shear force vs. depth profile was performed to acquire the profile of soil resistance  $p$ . It is illustrated as Eq. (3).

$$p = \frac{dV}{dz}, \tag{3}$$

where  $p$  = net soil resistance per unit length of piles; and  $V$  = shear force at a depth  $z$ .

A compiled MATLAB procedure was used to implement the above calculation process in which it referred to approximation and interpolation techniques. Figure 8a shows the shear force along the pile length extracted from numerical simulation results and fitted by 9th order polynomial. It implies that there exists a good agreement between fitting values and those obtained from calculation. Corresponding lateral soil resistance vs. depth curves for several different radiuses of grouting soil are presented in Fig. 8b.

### 6.2 Hyperbolic $p$ - $y$ Model for Gravel Soil

It is suggested that a  $p$ - $y$  curve model [17] for sand is used to fit considerably well for the data from model test results in the Nak-dong River sand. Thus, a hyperbolic  $p$ - $y$  model is decided to study the nonlinear response of the pile in improved gravel soil in this paper. This approach assumes soil medium as some discrete nonlinear springs supporting laterally loaded piles. Uncouple springs represents load transfer relationship between lateral deflection  $y$  of the pile

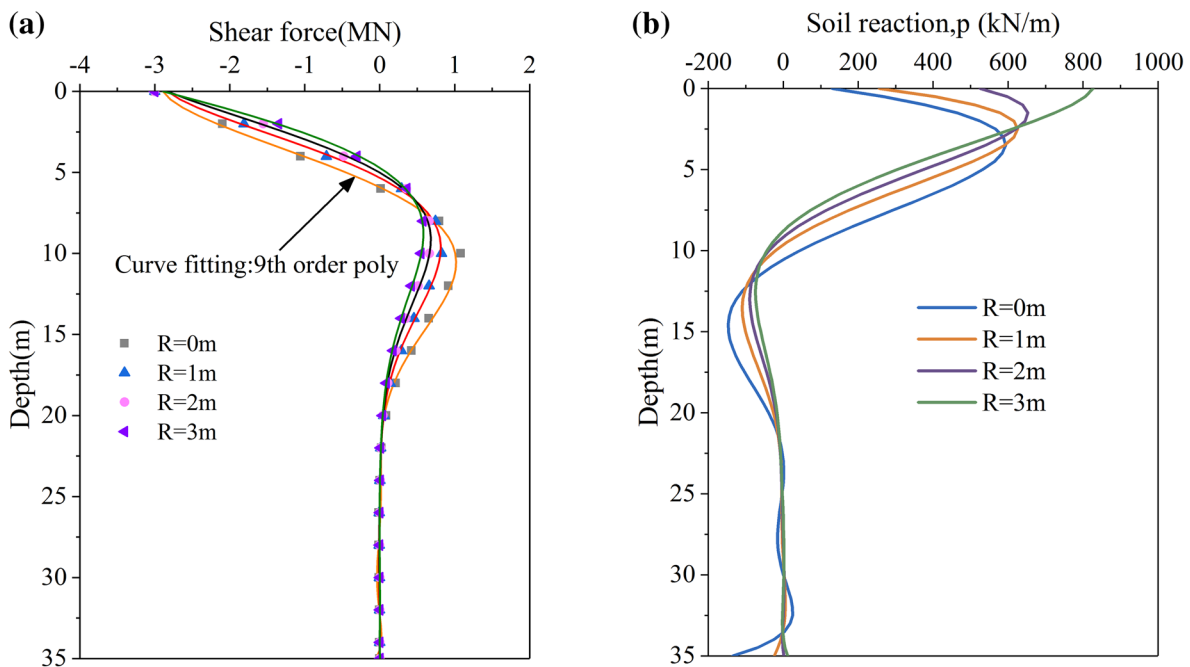


**Fig. 8** Response of internal force of pile under 3000 kN: **a** shear force of pile, **b** soil resistance for different range of grouting soil

at the position of the spring and the soil reaction  $p$ . Some typical back-analysis and fitted  $p$ - $y$  curves can be seen in Fig. 9. The following Eq. (4) is employed to illustrate  $p$ - $y$  curves:

$$p = \frac{y}{\frac{1}{k} + \frac{y}{p_u}}, \quad (4)$$

where  $k$  is the initial lateral subgrade reaction modulus from a mechanical point of view, it is also the initial slope of  $p$ - $y$  curves from the geometrical mean.  $p_u$  is ultimate soil resistance per unit length. The shape of the hyperbolic curve is decided by the two significant parameters  $k$ ,  $p_u$  which have been studied by many researchers.

#### 1. Proposed equation for initial lateral subgrade reaction modulus $k$

The effect of annular grouting radius is investigated by varying the radius from 0 to 3 m. Other correlative parameters are kept as invariable. The results of FEM are as shown in Fig. 10 describing there is an increasing linear relationship between normalized modulus of subgrade reaction and normalized annular grouting radius. We find an intercept which indicates initial subgrade reaction modulus in virgin soil at a specific depth for several linear function curves.

The correlation between initial subgrade reaction modulus and depth is also studied by extracting the data at the depth of 0.5–2.5 m. Other pertinent parameters are kept as constant. Liang [31] adopted a power function to match the relationship between initial subgrade reaction modulus of soil and depth. This function is also applied in this study to represent the link between grouting depth  $z$  and  $k$ . It can be seen from Fig. 11 that it is suitable to use a power function to achieve a goodness of fit with the data from numerical analysis.

The traditional theory assumes that the initial stiffness of a  $p$ - $y$  curve at a given depth increases with depth below the ground surface. However, as can be seen in Fig. 11, contrary to this understanding, the initial slope of  $p$ - $y$  in the cement-treated zone always surpasses one for the unimproved soil at the identical position and degrades as the depth increases. It is worthwhile to note that this phenomenon was also observed in the experimental  $p$ - $y$  curves on the left side of a centrifuge test of a single pile in the partly treated zone [8]. It might be because the initial subgrade reaction modulus is more affected by weak virgin soil below the improved gravel soil as the location increases along the depth. In other words, subsoil makes contribution to providing support and constraint to topsoil. The Relative stiffness of adjacent soil layers has a definite influence on upper soil's initial slope of  $p$ - $y$  curve to some extent.

Therefore, the initial lateral subgrade reaction modulus  $k$  increases linearly as the grouting radius of soil surrounding single pile gets larger. The initial lateral subgrade reaction modulus  $k$  presents a power relationship with depth of improved soil along pile length. A regression analysis on the data from numerical simulation parametric research is conducted in this study. The fitting result is presented in Fig. 12. An equation for predicting initial subgrade reaction modulus of improved soil is developed to match  $k$  values obtained from back-analysis parametric study via the finite element method. As shown in Eq. (5), the suggested equation can be expressed as follows:

$$k = 0.86E_s \cdot z^{-0.416} \sqrt{1.433 + 1.384 \frac{R}{R_{\text{ref}}}}, \quad (5)$$

where  $E_s$  means elastic modulus of virgin gravel soil, reference radius  $R_{\text{ref}}$  equals pile's radius, 1 m.

#### 2. Proposed equation for ultimate soil resistance $p_u$

The effect of annular grouting soil radius on ultimate soil resistance at a given location is reflected by a power function as shown in Fig. 13. There is a nonzero value at vertical coordinate when  $R$  equals zero, which stands for limit lateral soil resistance at the corresponding depth under the un-treated circumstance. The normalized ultimate soil resistance rises as grouting soil radius expands.

It is similar to the traditional theory that the limit lateral soil resistance has a power function with depth of grouting soil. As is shown in Fig. 14, it is appropriate to use a power function to reflect the relationship between numerical results and fitting results.

The ultimate soil resistance  $p_u$  increases in a power function as the grouting radius of soil surrounding the single pile and depth of improved soil along the pile length get larger. According to the results of the above regression analysis, an equation is established as shown in Eq. (6) to predict the effect of grouting in shallow layers on the ultimate lateral soil resistance. The fitting result is presented in Fig. 15.

$$p_u = \left( 1.318 + 0.63 \left( \frac{R}{R_{\text{ref}}} \right)^{0.88} \right) k_p^2 \gamma \left( \frac{z}{R_{\text{ref}}} \right)^{0.5} D, \quad (6)$$

where  $D$  is the pile diameter;  $\gamma$  is the effective unit weight of soil; reference radius  $R_{\text{ref}}$  equals pile's radius; coefficient of passive earth pressure  $k_p$  is related to the friction angle  $\phi$ , it can be expressed as follow:

$$k_p = \tan^2 \left( 45^\circ + \frac{\phi}{2} \right). \quad (7)$$



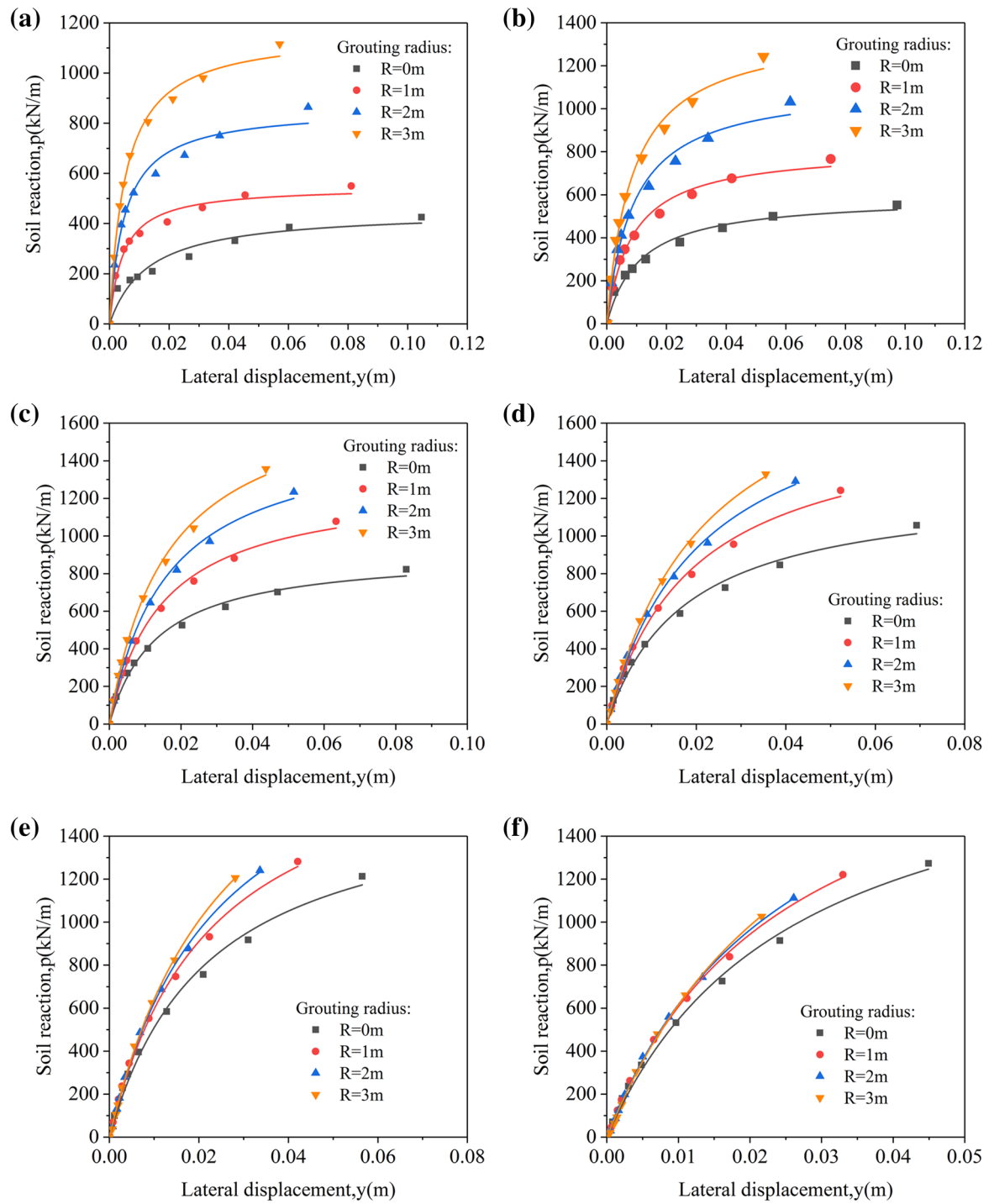


**Fig. 9** Comparison of  $p$ – $y$  curves: **a** depth = 0.5 m, **b** depth = 1.0 m, **c** depth = 2.0 m, **d** depth = 3.0 m, **e** depth = 4.0 m and **f** depth = 5.0 m

### 7 Case Study

A laterally loaded test was performed to study response of the single pile in virgin soil and improved soil in the upper portion of the soil surrounding the pile. Grain

size distribution of soil used in the test is presented in Fig. 16 to illustrate gravel soil’s composition as single layer soil. A 1/40 scale model of the bored concrete pile in the field test was pre-embed in the soil profile to model its behaviour as closed-ended steel-pipe piles. A steel

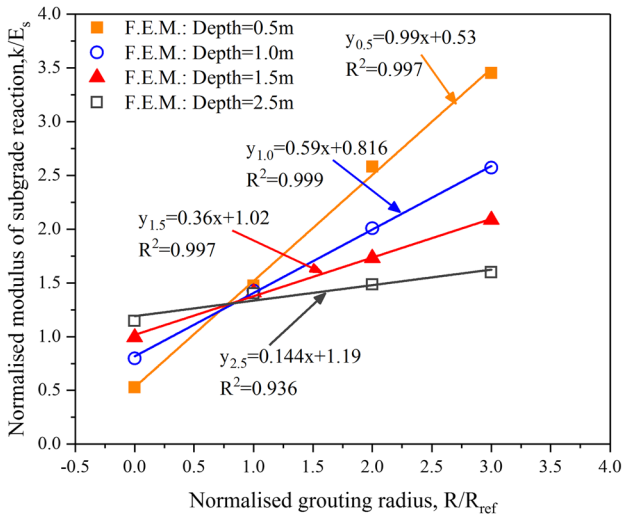


Fig. 10 Functional relationship between  $k$  and  $R$

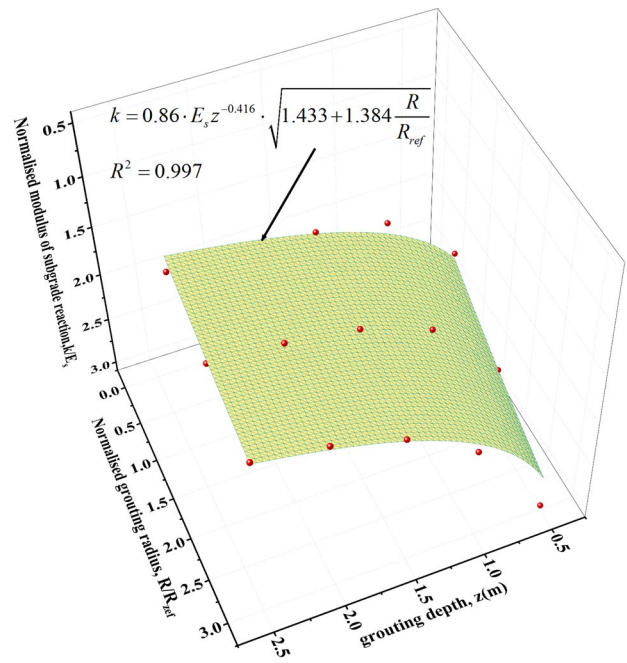


Fig. 12 Empirical functional of  $k$

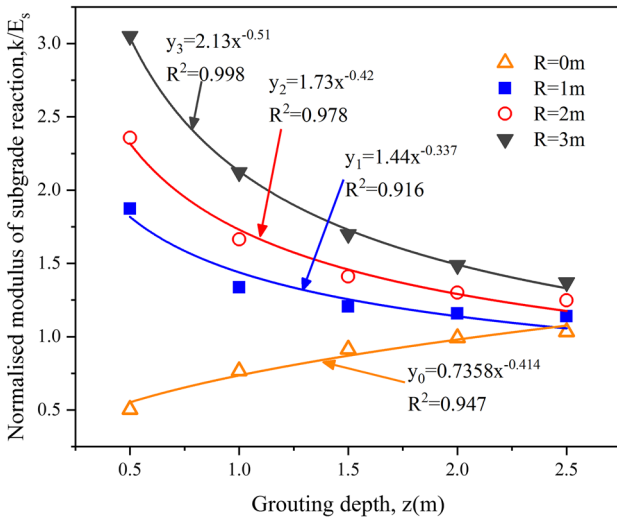


Fig. 11 Functional relationship between  $k$  and  $z$

pipe pile with the geometry as length  $\times$  diameter  $\times$  thickness = 0.95 m  $\times$  48 mm  $\times$  2.5 mm is shown in Fig. 17.

Gravel soil's natural unit weight is 21 kN/m<sup>3</sup>, and compression modulus is 8.3 MPa. Its friction angle is measured to be 39.8°. The upper portion of the soil surrounding the pile was cement-improved with depth and ring radius of three times the pile diameter. The strain gauges and YHD-100 type displacement sensor were measured by TDS-530 which is an automatic, multi-channel scanning data logger for reading strain gauges, thermocouples, Pt RTD temperature sensors, strain gauge based (full bridge) transducers and DC voltage.

To calibrate the flexural stiffness of steel pipe pile, a pure bending test of the simply supported beam was carried out

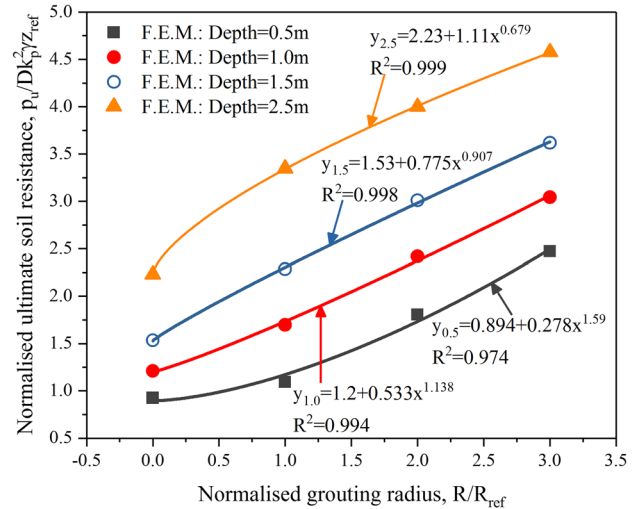


Fig. 13 Functional relationship between  $p_u$  and  $R$

to apply vertical load over the middle position of the pile. Gauge constants were computed for every gauge separately. The observed strain values and theoretical values of bending moment were correlated to calculate gauge constants which were decided by the method of least squares. The calibrated result is shown in Fig. 18. The pile and strain were observed during the calibration. The flexural stiffness  $EI$  is calculated to be 2.13e10 N m<sup>2</sup>, and the calibration coefficient is 0.1122 N m/ $\mu\epsilon$ .

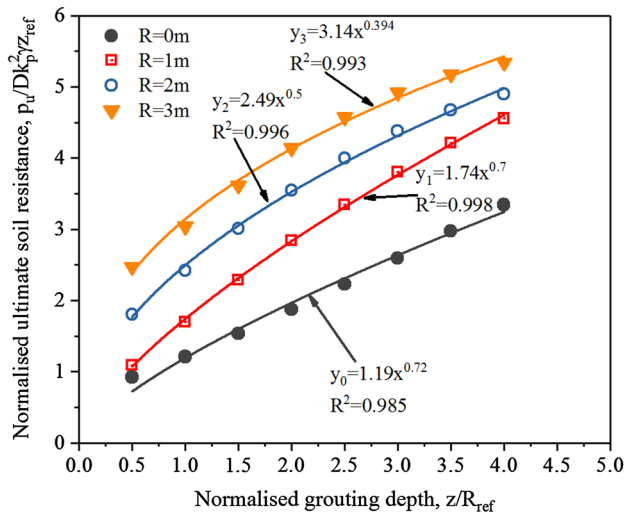


Fig. 14 Functional relationship between  $p_u$  and  $z$

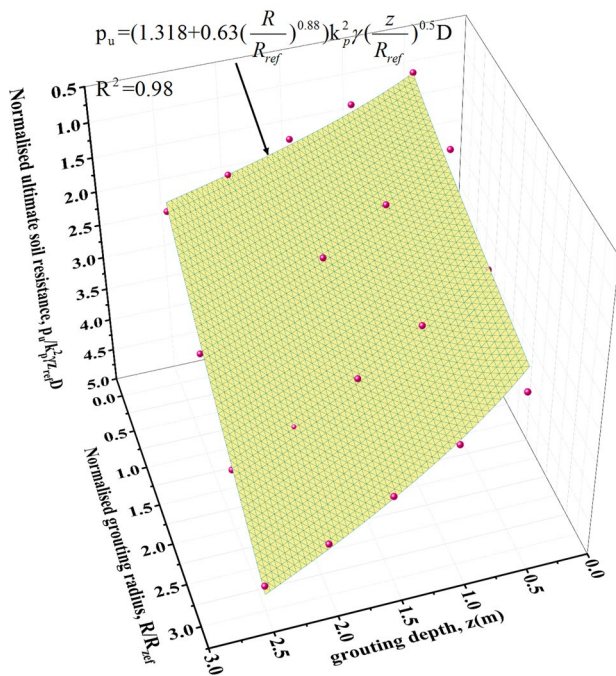


Fig. 15 Empirical functional of  $p_u$

Figure 19 shows the relationship between lateral load and deflection of the pile top obtained from measurement and the proposed method by Lpile computer program [32]. The  $p$ – $y$  curves measured in the model test were inputted into Lpile to calculate the relationship between load and displacement at the pile top in virgin soil. It can be shown in Fig. 19 that there is a good agreement between measured results and Lpile’s results. Therefore, the soil of  $3D$  in depth below ground surface was substituted by the hyperbolic  $p$ – $y$  model proposed in this paper to simulate the behaviour of

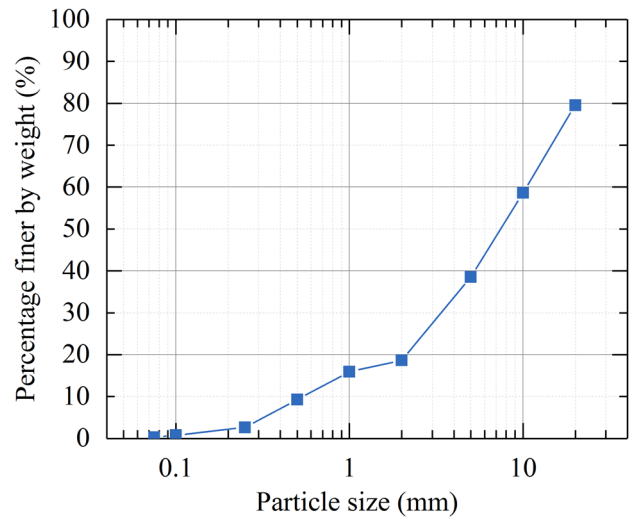


Fig. 16 Grain size distribution of soils at the model test

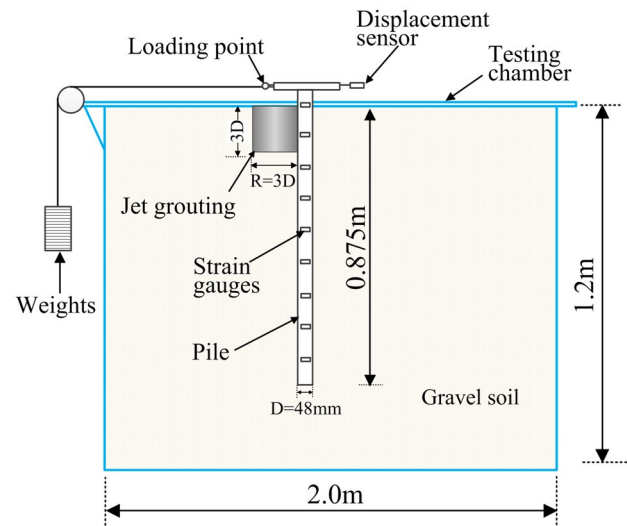
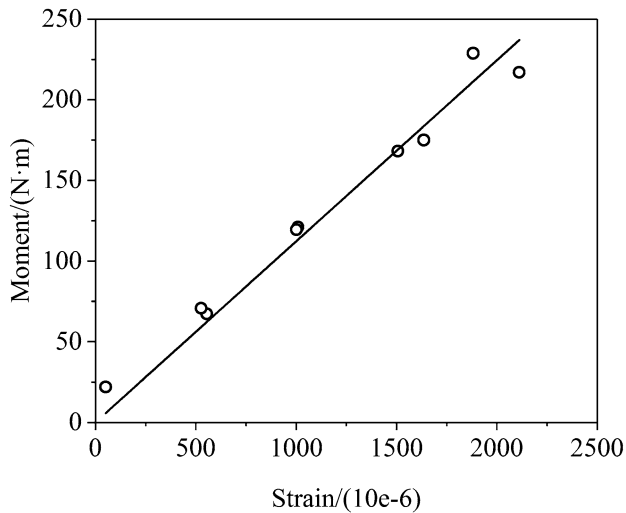


Fig. 17 Schematic of the experimental setup

cement-improved soil. The  $p$ – $y$  curves of virgin soil below improved soil are from measurement results. The calculated result with respect to the proposed method reflects well the response of the single pile pre-embedded in upper cement-improved soil.

Figure 20 shows the Bending moment along depth obtained from measurement, the proposed method by Lpile. The bending moments were measured by nine pairs of strain gauges attached to the inner steel pipe with a distance of 100 mm. In terms of the response of the single pile in virgin soil, it can be predicted well for the bending moment of pile subjected to the low-grade lateral load such as 0.4 kN and 0.8 kN. The measured  $p$ – $y$  curves have lower bending moments than measurement results



**Fig. 18** The relationship between measured strain and calculated moment

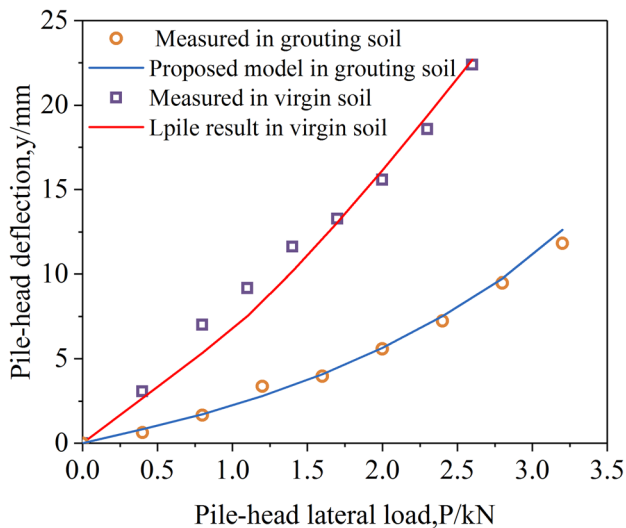


**Fig. 19** Load at the pile head vs. deflection at the pile head obtained by measurement, the proposed method and the *p-y* method from measurement result by Lpile

under 2.0 kN. This is likely because the flexural rigidity degrades with the load grade increasing, which is not considered in the computational process. It can be observed from Fig. 20b that the result of the proposed method is very close to the measuring bending moment of the single pile in improved soil. It is obvious that the pile's bending moments along depth reduce significantly under every loading level because the shallow soil profile is improved.

These results illustrate the effectivity of increasing the lateral soil resistance by cement-improving upper soil ahead

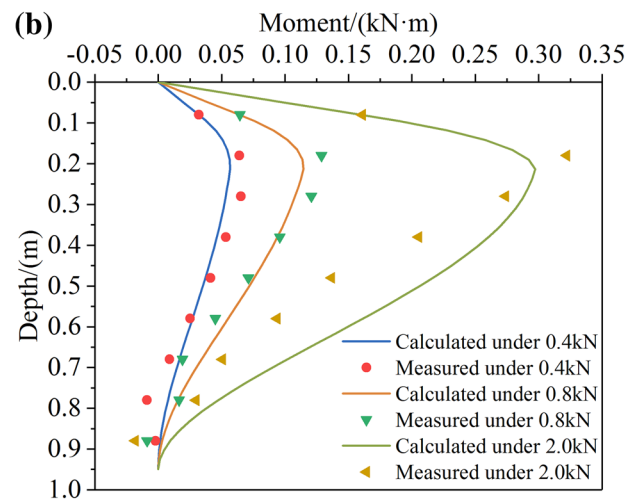
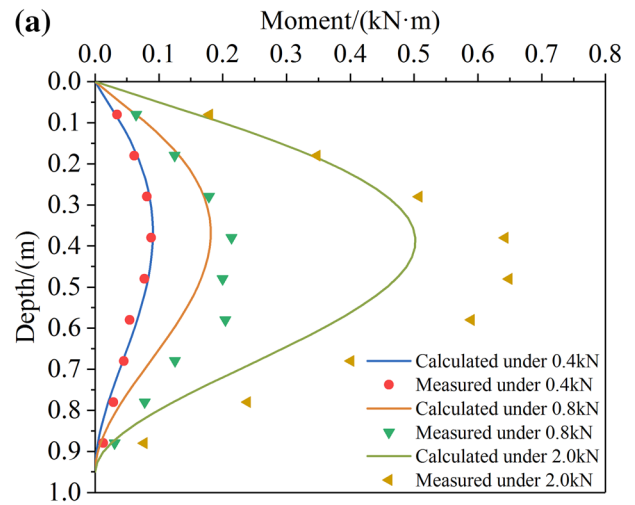


**Fig. 20** Bending moment along depth obtained by measurement, the proposed method and the *p-y* method from measurement result by Lpile: **a** pile in virgin soil and **b** pile in improved soil

of the pile. Both maximum bending moment and deformation of the single pile reduce because of cement-improved soil.

## 8 Conclusions

A field case study of high-pressure jet grouting technique applied to improve the upper portion of gravel soil ahead of a single pile to increase the lateral soil resistance is reported. The lateral deflection of piles in virgin soil and improved soil were observed. The software program PLAXIS3D version 2016 was used to simulate interaction between the pile and improved soil. Based on the observed and simulated results, the following conclusions can be drawn. They can

be used as a design guideline in practice in the case where the foundation is sensitive to lateral displacement.

1. The observed data show that the horizontal bearing capacity of single piles is increased by 43% in the case of cement-improved gravel soil. It is an available method to increase the lateral soil resistance by cement-improving shallow soil ahead of the pile.
2. The coincidence between measuring and simulating results shows that it is reasonable to use a non-associated Mohr–Coulomb model to reflect the behaviour of improved soil in the field test. Both strength and stiffness of subsoil are enhanced by jet grouting technique.
3. The improved gravel soil ahead of the pile provides lateral resistance with better integrity than virgin soil does due to its cohesion and friction angle increased. More soils at the side of the pile are involved in the area resisting lateral loads under the action of adjacent soil. The contribution of shallow soil behind the pile to lateral soil resistance do not increase because of the gap between the pile and soil.
4. By taking full account of the 3D, nonlinear interaction between improved gravel soil and the pile, the proposed  $p$ – $y$  curve is a reasonable representation of the lateral load-transfer characteristics of flexible piles in cement-improved soil. The fact that calculated results are close to model test results suggests that the proposed method can predict well the behaviour of the pile subjected to lateral loads in shallow gravel soil improved. The proposed  $p$ – $y$  curve's shape is completely controlled by initial lateral subgrade reaction modulus and the ultimate soil resistance.

**Acknowledgements** The authors gratefully acknowledge the financial support of the National Key Research Program of China (2017YFC0703408) and National Natural Science Foundation of China (51678145). These financial supports are gratefully acknowledged.

**Funding** The research work is supported by National Key Research Program of China (2017YFC0703408) and National Natural Science Foundation of China (51678145).

## References

1. Zhong R, Huang M (2013) Winkler model for dynamic response of composite caisson-piles foundations: lateral response. *Soil Dyn Earthq Eng* 55:182–194
2. Gong W, Wang L, Yin Y, Tong X (2013) Experimental study on horizontal bearing capacity of root-caisson foundation. *China Build Struct* 43:90–94
3. Ashford SA, Rollins KM, Baez JI (2000) Comparison of deep foundation performance in improved and non-improved ground using blast-induced liquefaction. In: *Soil dynamics and liquefaction*, pp 20–34
4. Rollins KM, Sparks A (2002) Lateral resistance of full-scale pile cap with gravel backfill. *J Geotech Geoenviron Eng* 128(9):711–723
5. Rollins KM, Snyder JL, Walsh JM (2010) Increased lateral resistance of pile group in clay using compacted fill. In: *GeoFlorida 2010: advances in analysis, modeling and design*, pp 1602–1611
6. Rollins KM, Herbst M, Adsero M, Brown D (2010) Jet grouting and soil mixing for increased lateral pile group resistance. In: *GeoFlorida 2010: advances in analysis, modeling and design*, pp 1563–1572
7. Rollins KM, Brown DA (2011) Design guidelines for increasing the lateral resistance of highway-bridge pile foundations by improving weak soils, vol 697. Transportation Research Board, Washington, DC
8. Soltani H, Muraleetharan KK (2015) Experimental  $p$ – $y$  curves for a laterally loaded single pile in cement-improved soft clay. In: *IFCEE*, pp 1122–1131
9. Taghavi A, Muraleetharan KK, Miller GA, Cerato AB (2015) Centrifuge modeling of laterally loaded pile groups in improved soft clay. *J Geotech Geoenviron Eng* 142(4):04015099
10. Taghavi A, Muraleetharan KK, Miller GA (2017) Nonlinear seismic behaviour of pile groups in cement-improved soft clay. *Soil Dyn Earthq Eng* 99:189–202
11. Sharafi H, Sojoudi Y (2016) Experimental and numerical study of pile-stabilized slopes under surface load conditions. *Int J Civ Eng* 14(4):221–232. <https://doi.org/10.1007/s40999-016-0017-2>
12. Reese LC, Matlock H (1956) Non-dimensional solutions for laterally-loaded piles with soil modulus assumed proportional to depth. In: *Association of drilled shaft contractors*
13. Hetényi M (1971) Beams on elastic foundation: theory with applications in the fields of civil and mechanical engineering. University of Michigan, Ann Arbor
14. Matlock H (1970) Correlations for design of laterally loaded piles in soft clay. In: *Offshore technology in civil engineering's hall of fame papers from the early years*, pp 77–94
15. Reese LC, Cox WR, Koop FD (1974) Analysis of laterally loaded piles in sand. In: *Offshore technology in civil engineering hall of fame papers from the early years*, pp 95–105
16. Tak Kim B, Kim NK, Lee J, Kim W, Su Y (2004) Experimental load–transfer curves of laterally loaded piles in Nak-Dong River sand. *J Geotech Geoenviron Eng* 130(4):416–425
17. Kondner RL (1963) Hyperbolic stress-strain response: cohesive soils. *J Geotech Eng Div* 89(1):115–143
18. Norske Veritas D (1977) Rules for the design, construction and inspection of offshore structures, appendix F, Foundations. Det norske Veritas, Høvik
19. Scott R (1980) Analysis of centrifuge pile tests: simulation of pile-driving. Research Report, API OSPAR Project 13, California Institute of Technology, Pasadena
20. Norris GM (1986) Theoretically based BEF laterally loaded pile analysis. In: *Proceedings of the 3rd international conference on numerical methods in offshore piling*, Navtes, pp 361–386
21. Murchison JM, O'Neill MW (1984) Evaluation of  $p$ – $y$  relationships in cohesionless soils. In: *Analysis and design of pile foundations*. ASCE, pp 174–191
22. Wesselink BD, Murff JD, Randolph MF, Nunez IL, Hyden AM (1988) Analysis of centrifuge model test data from laterally loaded piles in calcareous sand. *Eng Calcareous Sediments* 1:261–270
23. Faro VP, Consoli NC, Schnaid F, Thomé A, da Silva Lopes L (2015) Field tests on laterally loaded rigid piles in cement treated soils. *J Geotech Geoenviron Eng* 141(6):06015003
24. Kim Y, Jeong S (2011) Analysis of soil resistance on laterally loaded piles based on 3D soil–pile interaction. *Comput Geotech* 38(2):248–257

25. Comodromos EM, Papadopoulou MC, Rentzeperis IK (2009) Pile foundation analysis and design using experimental data and 3-D numerical analysis. *Comput Geotech* 36(5):819–836
26. Wallace JW, Fox PJ, Stewart JP, Janoyan K, Qiu T, Lermite S (2001) Cyclic large deflection testing of shaft bridges: part I—background and field test results. Report to California Department of Transportation
27. Poulos HG, Davis EH (1980) Pile foundation analysis and design (no. monograph)
28. Taghavi A, Muraleetharan KK (2016) Analysis of laterally loaded pile groups in improved soft clay. *Int J Geomech* 17(4):04016098
29. Han F, Salgado R, Prezzi M (2015) Nonlinear analyses of laterally loaded piles—a semi-analytical approach. *Comput Geotech* 70:116–129
30. Haiderali AE, Madabhushi G (2016) Evaluation of curve fitting techniques in deriving  $p$ - $y$  curves for laterally loaded piles. *Geotech Geol Eng* 34(5):1453–1473
31. Liang R, Shatnawi ES, Nusairat J (2007) Hyperbolic  $p$ - $y$  criterion for cohesive soils. *Jordan J Civ Eng* 1(1):38–58
32. Reese LC, Wang ST, Isenhower WM, Arréllaga JA, Handrix J (2000) LPILE plus 4.0—a program for the analysis of piles and drilled shafts under lateral loads. Ensoft Inc., Austin